AD-A194 066 THREE-DIMENSIONAL VORTEX INTERACTIONS(U) MCDONNELL 1/1
DOUGLAS RESEARCH LABS ST LOUIS MO V KIBENS ET AL.
15 JAN 88 MDC-QA005 AFOSR-TR-88-0484 F49620-86-C-0090
UNCLASSIFIED F/G 20/4 NL

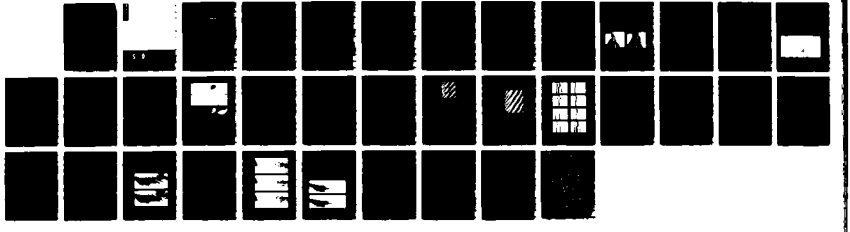

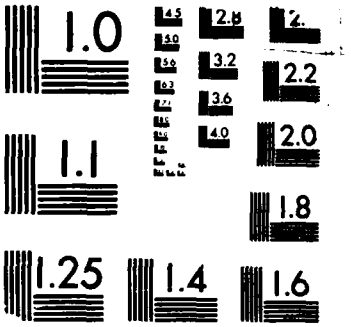

MICROCOPY RESOLUTION TEST CHART

BUREAU OF STANDARDS-1963-A

McDonnell Douglas Research Laboratories

UNCLASSIFIED
SECURITY CLASSIFICATION OF THIS PAGE

ADA194066

REPORT DOCUMENTATION PAGE

1a. REPORT SECURITY CLASSIFICATION Unclassified	1b. RESTRICTIVE MARKINGS
2a. SECURITY CLASSIFICATION AUTHORITY	3. DISTRIBUTION/AVAILABILITY OF REPORT Approved for public release; distribution unlimited
2b. DECLASSIFICATION/DOWNGRADING SCHEDULE	
4. PERFORMING ORGANIZATION REPORT NUMBER(S) MDC QA005	5. MONITORING ORGANIZATION REPORT NUMBER(S) AFOSR-TR- 88-0484
6a. NAME OF PERFORMING ORGANIZATION McDonnell Douglas Research Laboratories 6b. OFFICE SYMBOL (If applicable)	7a. NAME OF MONITORING ORGANIZATION AFOSR/NA
6c. ADDRESS (City, State, and ZIP Code) P. O. Box 516 St. Louis, MO 63166	7b. ADDRESS (City, State, and ZIP Code) Bolling Air Force Base Washington, DC 20332
8a. NAME OF FUNDING/SPONSORING ORGANIZATION Department of the Air Force 8b. OFFICE SYMBOL (If applicable) AFOSR/NA	9. PROCUREMENT INSTRUMENT IDENTIFICATION NUMBER F49620-86-C-0090DEF
8c. ADDRESS (City, State, and ZIP Code) Air Force Office of Scientific Research/AFOSR Bolling Air Force Base Washington, DC 20332	10. SOURCE OF FUNDING NUMBERS PROGRAM ELEMENT NO. 61102F; PROJECT NO. 2307; TASK NO. A2; WORK UNIT ACCESSION NO.
11. TITLE (Include Security Classification) Three-Dimensional Vortex Interactions	
12. PERSONAL AUTHOR(S) Kibens, Valdis; Wlezien, Richard W.; Roos, Frederick W.; and Kegelman, Jerome T.	
13a. TYPE OF REPORT Annual Technical 13b. TIME COVERED FROM 86 Sep 1 TO 87Aug31	14. DATE OF REPORT (Year, Month, Day) 1988 January 15 15. PAGE COUNT 34
16. SUPPLEMENTARY NOTATION	

17. COSATI CODES			18. SUBJECT TERMS (Continue on reverse if necessary and identify by block number)		
FIELD	GROUP	SUB-GROUP	Fluid mechanics	Passive control	Control of turbulence
			Shear layers	Active control	Asymmetric nozzles
			Jet flows	Image processing	Slanted nozzles

19. ABSTRACT (Continue on reverse if necessary and identify by block number)

Three-dimensional vortex interactions were investigated in jets with slanted, indeterminate origin exit nozzles, and in mixing layers behind a splitter plate with a swept trailing edge. Flow visualization images were quantitatively processed to characterize complex three-dimensional vortex interactions in nonaxisymmetric jets. Phase conditioned pulsed laser-sheet illumination was used to obtain a series of sectional images while rotating the asymmetric nozzle. The sectional images were recombined into an unwrapped representation of the developing vortex systems in the shear layer. Partial pairing of sections of adjacent vortex systems was shown to be responsible for asymmetric shear layer growth. Flow visualization in the flow behind the swept trailing edge showed that two families of instability waves can develop with different orientations with respect to the trailing-edge angle. Excitation was shown to enhance waves with orientation parallel to the trailing edge or perpendicular to the mean flow direction, depending on excitation frequency. Streamwise wavelengths of the two wave families were related by their angular separation. Keywords:

20. DISTRIBUTION/AVAILABILITY OF ABSTRACT ☐ UNCLASSIFIED/UNLIMITED ☒ SAME AS RPT ☐ DTIC USERS	21. ABSTRACT SECURITY CLASSIFICATION Unclassified
22a. NAME OF RESPONSIBLE INDIVIDUAL James M. McMichael	22b. TELEPHONE (Include Area Code) (202) 767-4935 22c. OFFICE SYMBOL AFOSR/NA

DD FORM 1473, 84 MAR 83 APR edition may be used until exhausted. All other editions are obsolete

SECURITY CLASSIFICATION OF THIS PAGE
UNCLASSIFIED

18. SUBJECT TERMS - Continued

Indeterminate origin nozzles
Pulsed laser flow visualization
Mixing layers
Instability waves

PREFACE

The work reported herein was performed by the McDonnell Douglas Research Laboratories in St. Louis, Missouri, for the United States Air Force Office of Scientific Research, Bolling Air Force Base, Washington, DC, under Contract F49620-86-C-0090DEF. The work reported was conducted from 1 September 1986 to 31 August 1987 in the Flight Sciences Department, managed by Dr. R. J. Hakkinen. The principal investigator was Dr. V. Kibens. Co-investigators were Dr. R. W. Wlezien, Dr. F. W. Roos, and Dr. J. T. Kegelman.

This technical report has been reviewed and approved.

R. J. Hakkinen
Director-Research, Flight Sciences
McDonnell Douglas Research Laboratories

D. P. Ames
MDC Distinguished Fellow -
General Manager
McDonnell Douglas Research Laboratories

TABLE OF CONTENTS

LIST OF ILLUSTRATIONS

1. INTRODUCTION

Efficient turbulence control techniques applied to unsteady flowfield phenomena are needed to optimize operation of aerodynamic and propulsion systems. Manipulation of three-dimensional vortex flowfields is central to such techniques. The work reported herein approaches the investigation of three-dimensional vortex systems in two stages. The first stage involves the use of high-resolution, high-data-rate instrumentation and data processing to extricate the specifics of three-dimensional coherent motion from the background of random turbulence and to describe the interaction of the vortex systems that comprise that motion. This stage is being performed in indeterminate origin (I.O.) nozzle flows. The second stage consists of the investigation of the simplest shear-layer vortex systems that retain elementary features of three-dimensionality, and is being performed in a two-dimensional shear layer behind a plate with a swept trailing edge.

The work described in this report covers the results obtained during the first year of a two-year program.

2. OBJECTIVES

The principal objectives of the program are the following:

A. Investigate the nature and controllability of fundamental three-dimensional vortex interactions in the shear layer of free jets issuing from indeterminate-origin nozzles by

(1) experimentally determining, for selected nozzles, the onset and evolution of three-dimensional interactions between organized vortex structures developing from basic shear layer instabilities under natural and forced excitation by use of scanning laser illumination and phase-conditioned video image-processing techniques together with laser-Doppler and hot-wire velocimetry,

(2) conducting suitable calibration procedures to permit reliable correlation between scattered-light intensity maxima and flowfield vorticity,

(3) developing algorithms for evaluating mass entrainment and directional spreading rates of the jet flowfield by use of processed flow-visualization data,

(4) initiating feedback control investigations using suitable flowfield sensors that drive single- or multiple-sector exciters.

B. Investigate elementary three-dimensional vortex interactions in the free shear layer between two air streams of different speeds downstream of a splitter plate with a swept trailing edge by

(1) setting up a suitable splitter plate apparatus with an electromechanical excitation system allowing segmented excitation of the shear layer near the trailing edge,

(2) conducting flow visualization and image processing as in Section A to identify coherent regions of vorticity and their three-dimensional interactions,

(3) varying the splitter plate sweep angle and excitation waveforms to determine their effect on vortex interactions.

3. DESCRIPTION OF VORTEX INTERACTIONS

3.1 Background:

In previous work, under AFOSR Contract No. F49620-83-C-0048, the development of plumes from initially nonaxisymmetric nozzles was investigated (References 1 and 2). In unexcited jets, the shear-layer instability-wave system was shown to undergo complex three-dimensional interactions which produce strong asymmetry in shear-layer spreading rates, and an overall net increase in jet spreading. Acoustic excitation was shown to produce an even wider range of shear-layer responses, as well as stronger asymmetry. The excited nonaxisymmetric jets have highly three-dimensional but strictly repetitive vortex systems, which are typified in Figure 1. In this case, the nozzle exit is inclined and the jet is acoustically excited at a subharmonic of the shear-layer instability frequency.

Fig. 1 Complex shear-layer development in acoustically excited jet from inclined nozzle; $U_j = 30$ m/s; compound excitation at 1100 and 550 Hz; (a) and (b) at same relative phase.

The two schlieren visualization pictures [Figure 1(a) and (b)] illustrate the highly repetitive nature of the shear-layer structure, and indicate the existence of strong asymmetry in the vortex-pairing process. It is not possible to determine the details of the interaction mechanism from these images, however, because the schlieren process integrates the refraction of a light

beam traversing the entire flowfield. Furthermore, the helium tracer diffuses rapidly, making visualization difficult beyond the first several diameters of plume development. A quasi-quantitative technique was needed for characterizing the three-dimensional structure of vortex systems in these jets.

Techniques such as computed tomography were considered for processing the schlieren images. The requirements of low-noise images and multiple viewing angles makes the practical implementation of tomography difficult. Scanning-laser-sheet techniques (Reference 3) have been successfully used in low-speed flows, but laser pulse rates and image-recording rates are much too slow to be used in 30 m/s jets. The periodicity of an acoustically excited plume permits phase averaging with standard video and laser technology. Image processing was used to convert the laser-sheet images into a multidimensional description of the jet instability-wave system. A detailed set of laser Doppler velocimeter (LDV) data was also used to validate the flow-visualization technique.

3.2 Approach:

The nonaxisymmetric nozzle configuration used in this investigation is based on the indeterminate-origin nozzles described in Reference 1. A constant-diameter (d = 25.4 mm) extension was mounted at the exit of a contraction section. The tube was nominally 2.5 d in length, with an inclined exit of length d/2. Maintaining the convention adopted in References 1 and 2, we define the origin of the cylindrical coordinate system relative to the average axial location of the nozzle lip, with the reference azimuth angle $\psi = 0$ corresponding to the point on the nozzle extending farthest downstream.

The nozzle was mounted on the flow system by use of an indexing adaptor that allowed the nozzle to be rotated to an arbitrary azimuth relative to the stationary laser sheet. The flow system consists of a muffler, a low-angle conical diffuser, a settling chamber with honeycomb and screens, and tandem contraction sections with contraction ratios of 23:1 and 6.25:1. An electronically controlled blower provides a stable, quiet flow source. With appropriate measures taken to minimize blade-passing and system resonance frequencies, the irrotational low-frequency surging at the nozzle exit plane is less than 0.15% at an exit velocity of 30 m/s. The centerline turbulence intensity, as determined by two-sensor correlations, is 0.03%.

The shear layer was made visible by injecting atomized seed material into the boundary layer immediately upstream of the final contraction. A laser velocimetry seeding system was used to disperse 1-μm-diameter droplets of polyethylene glycol. A circular slit was used to inject the tracer nearly parallel to the mean flow with minimal disturbance to the jet. Four tubes around the periphery of the injection plenum were used to supply the tracer.

A 10-W pulsed copper-vapor laser system was used to selectively illuminate planes within the jet flowfield. The optical configuration (Figure 2) included a cylindrical lens to diverge the beam in the vertical direction, and a 1.6-m focal length parabolic mirror to focus the light into a sheet. The focal length of the mirror was chosen to be sufficiently long to provide a thin light sheet over the region of interest within the jet. For the present investigation, the light sheet was aligned vertically through the jet axis.

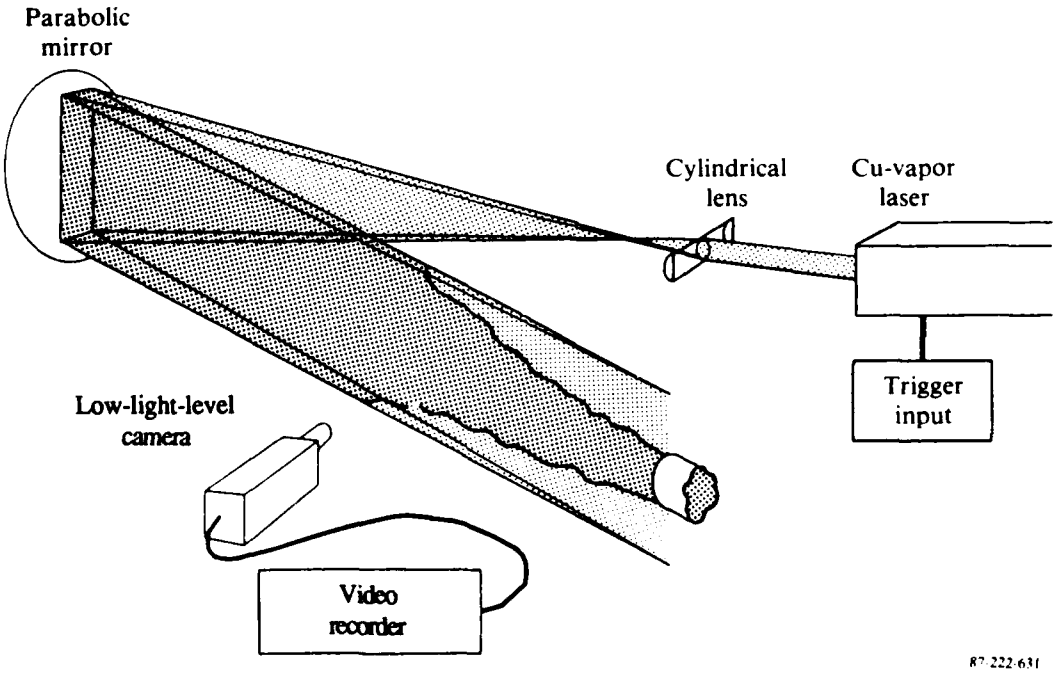

Fig. 2 Pulsed-laser flow-visualization configuration.

The illuminated flow was imaged by an RCA Ultricon low-light-level camera. This camera is sufficiently sensitive to produce usable images even when the flow is not visible to the unaided eye. The images were stored on videotape by a broadcast-quality video recorder.

The copper-vapor laser typically flashes at a repetition rate of approximately 6 kHz with a pulse duration of approximately 10 ns. The pulses were synchronized with the lowest subharmonic frequency of the excited jet (approximately 400 Hz) to produce phase-averaged images of the flow. It is possible to operate the laser at such low frequencies for only approximately one minute; at that time the plasma becomes sufficiently cool to prevent lasing. No attempt was made to synchronize the laser with the video camera. The persistence of the low-light-level camera was sufficient to smooth the 6-7 laser pulses that occurred in each video field. A computer-controlled delay was applied to the laser trigger signal to permit visualization at an arbitrary phase. A typical data run consisted of 2-s segments, each at constant phase, with the computer-controlled delay cycling through 32 segments of one cycle of the acoustic excitation. The high sensitivity of the camera coupled with the intense laser illumination produced high-contrast images at jet velocities in excess of 30 m/s. A typical digitized and enhanced image of an excited plume is shown in Figure 3.

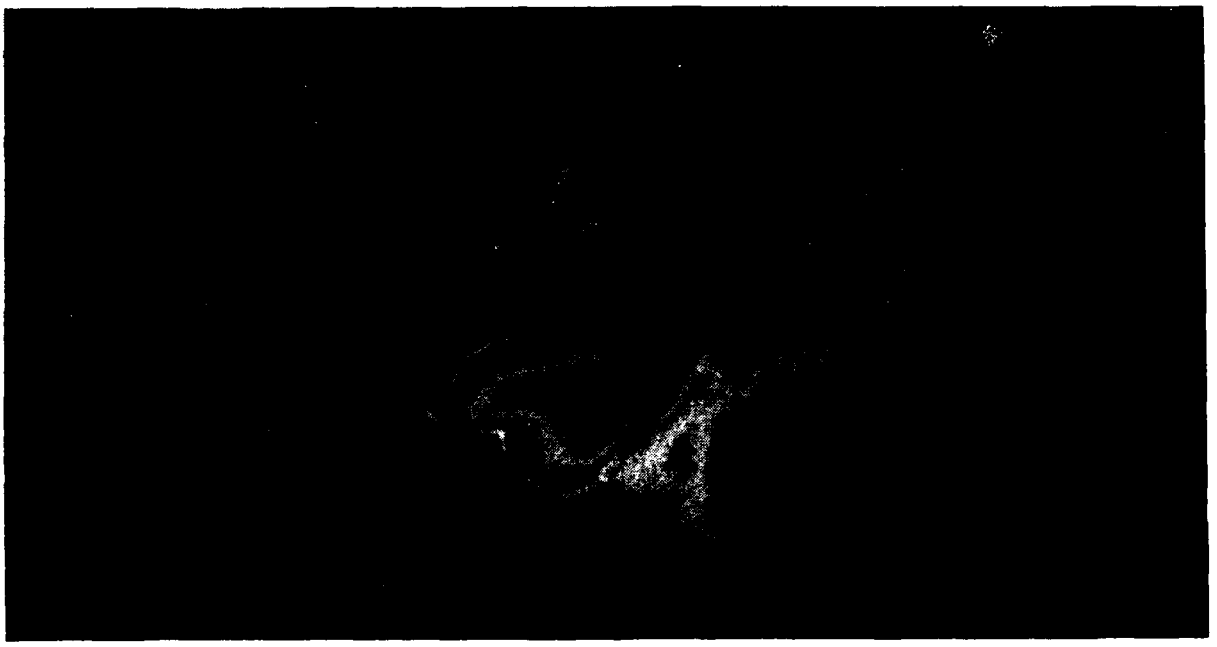

87-222-633

Fig. 3 Digitized pulsed-laser visualization of jet from inclined nozzle; $U_j = 30$ m/s; composite excitation.

A composite acoustic excitation scheme (Figure 4) was used to regularize the jet structure and to provide a phase reference for the conditionally averaged images. The fundamental excitation frequency, $f_0/2$ = 1526 Hz, corresponds to the first subharmonic of the shear-layer instability frequency at a jet exit velocity U_j = 30 m/s. The second subharmonic frequency $f_0/4$ is linearly added at a relative amplitude of 0.5 and an appropriate phase to spatially fix the vortex-pairing locations. The simple sum of these two frequencies is sufficient to induce a further coalescence at a frequency of $f_0/8$, the jet instability frequency. Frequency modulation with an amplitude of 10% at the $f_0/8$ subharmonic is sufficient to provide a stable phase lock. The composite excitation signal was computed and synthesized by use of an arbitrary waveform generator with a 64-bin resolution, a continuously adjustable master clock signal to tune the excitation, and low-pass filtering to remove higher harmonics generated by bin-to-bin discontinuities. Acoustic excitation was introduced to the flow through a high-frequency driver coupled to the flow-system plenum.

LDV measurements required a total of four days of acquisition time with precisely controlled jet characteristics. The excitation waveform illustrated in Figure 4 provided the greatest long-term stability for the flowfield, and was used for the detailed two-component, phase-conditioned LDV measurements. The flow-visualization measurements, which were performed earlier, did not require that excitation be matched so precisely to the shear-layer instability frequency. In that case only two frequencies were used in the multimode excitation, with components at 1100 Hz, the $f_0/3$ subharmonic of the shear-layer instability frequency, and the $f_0/6$ subharmonic, 550 Hz. Although use of this excitation scheme did not permit a direct comparison between the LDV and visualization data, qualitative similarity between the results can be demonstrated.

The initial digitization and centroid tracking of the flow-visualization images was conducted at the McDonnell Douglas Astronautics Company Image Processing Laboratory using a Gould 8500 image-processing system and a VAX 780 host. Two-second conditionally averaged images were acquired from the video and stored in 512 by 256 pixel by 8-bit format. The image enhancement and centroid tracking algorithms were developed on the host computer.

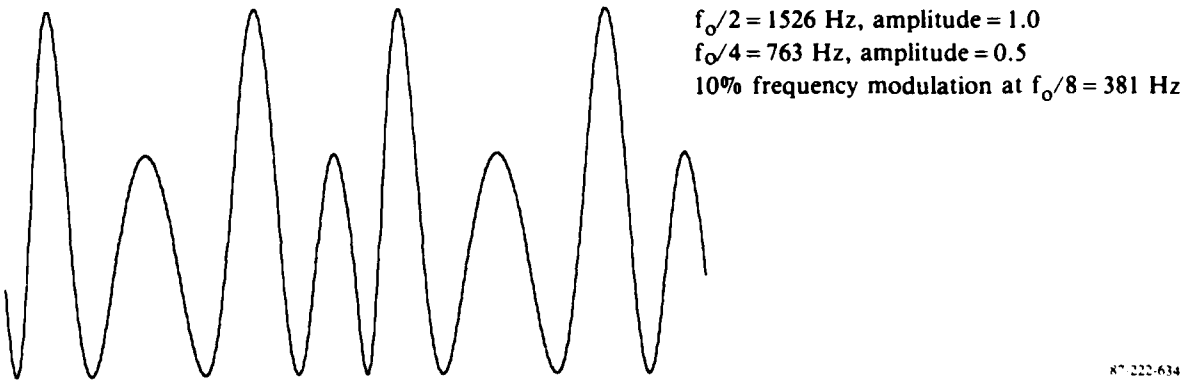

Fig. 4 Composite excitation signal.

Subsequent processing and analysis were conducted on the McDonnell Douglas Research Laboratories (MDRL) image-processing system. The system (Figure 5) is based on an Imaging Technologies ITI 200 image processor, and is hosted by a microVAX II minicomputer. The host has substantial mass storage and tape archiving capability, with the majority of processing functions conducted within the image processor. The ITI 200 is capable of digitizing and displaying images, with pipeline and pixel processors for image analysis. Four high-speed image buses permit real-time processing of video data.

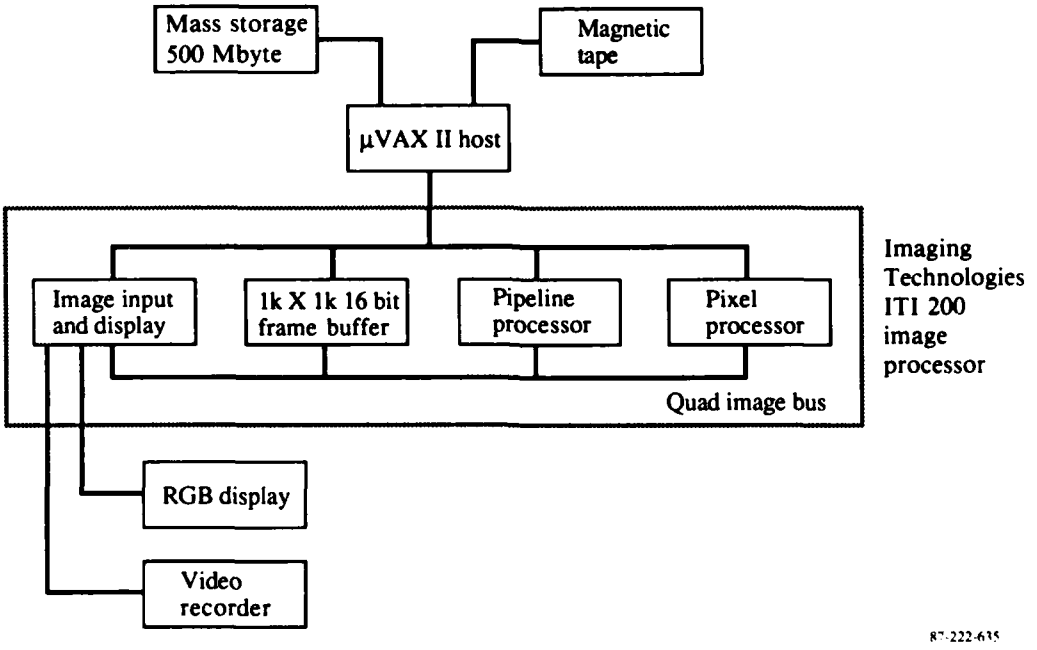

Fig. 5 Image-processing system.

3.3 Results and Discussion:

One period of the jet instability cycle was subdivided into 32 phases, and phase-conditioned images were obtained for ten azimuths to fully characterize the complex three-dimensional vortex field. The nozzle was rotated from 0 to 90 degrees in 10-degree increments relative to the stationary laser sheet. Upper and lower sections of the shear layer were simultaneously imaged, and symmetry was used to provide the remaining segments. Thus, approximately 42 Mbytes of raw image data were generated at a single flow condition.

Two techniques for tracking the vortex systems were developed. The first, referred to as adaptive centroid tracking, consists of image enhancement, thresholding, segmentation, and centroid detection. A more robust algorithm consists of radial integration, which is much less sensitive to random variations in image intensity and tracer distribution. Corroborative phase-conditioned vorticity measurements were used to verify the validity of the visualization techniques.

A typical digitized phase-averaged image of a laser-illuminated shear layer is shown in Figure 6(a). The picture is taken from a false-color image of the jet, and therefore grey-scale intensity does not accurately represent smoke concentration. The objective of the tracking algorithm is to segment the image into domains representing vorticity concentrations and to compute the centroids of the segmented regions to track vortex locations. A direct thresholding technique cannot be used because the image contrast varies with distance from the nozzle. Concentration of smoke in the initial segment of the shear layer is sufficiently dense to saturate the digitized image. Subsequent diffusion of the smoke produces significantly lower contrast at the end of the jet potential core. Simple compensation techniques for modeling tracer diffusion and linear jet-growth have limited success because of saturation and nonlinearities in the imaging system.

A local histogram equalization technique was used to create uniform contrast across an image. The initial contrast equalization is performed over the entire image domain; it maximizes image contrast near the nozzle exit, but does not provide sufficient contrast beyond the first pairing location. The second equalization pass is performed over the entire domain except the segment of the image near the nozzle exit; subsequent passes are performed over domains of decreasing streamwise extent, but including the downstream end of

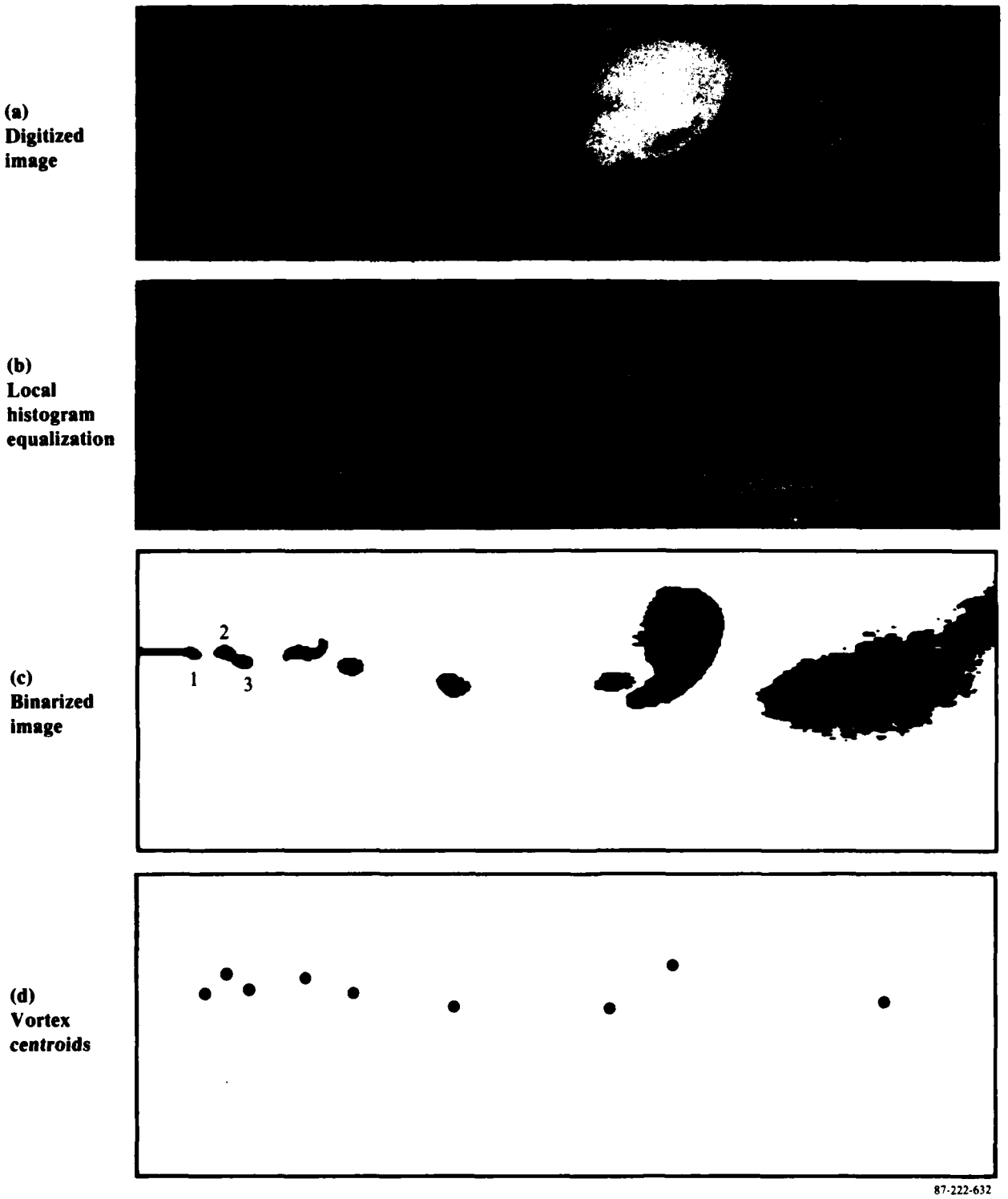

Fig. 6 Vortex tracking through enhancement, segmentation, and centroid computation.

the image. The result of the iterated equalization is an image of uniform contrast, Figure 6(b). Direct thresholding of the equalized image produces segmented domains [Figure 6(c)] for which the centroids can be directly computed.

The direct approach to vortex tracking described above suffers from two flaws that are difficult to overcome. First, the thresholds are arbitrarily chosen, and their levels vary with background illumination, laser intensity, and seed particle concentration. Manual intervention is required to determine an appropriate threshold to detect domains corresponding to vorticity concentrations. Second, a somewhat more difficult problem is posed by the need to separate domains that remain connected after thresholding. Successive erosion passes can be used to remove stray edge pixels, but the region labeled 1 in Figure 6(c) remains connected to the initial segment of the shear layer. Regions 2 and 3 are clearly two vortices about to merge, but the algorithm identifies them as a single entity.

An adaptive thresholding technique was developed to obtain the centroids shown in Figure 6(d) without making the tracking algorithm more arbitrary.

A schematic of adaptive thresholding is shown in Figure 7. A three-dimensional representation of the intensity distribution in a typical image illustrates the connected islands of intensity that correspond to discrete vortices. The difficulties associated with a single threshold level are clear. A threshold greater than 3 will not detect the leftmost peak, whereas a lower threshold will not separate the other two peaks.

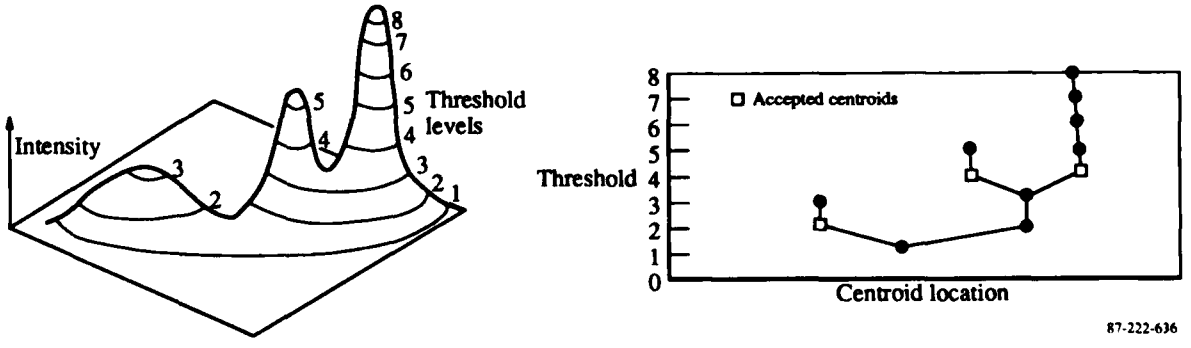

Fig. 7 Adaptive thresholding of images containing vortex signatures.

Adaptive thresholding begins with a maximal threshold level, which in the example of Figure 7 is a level of 8. The centroids of all detected domains are computed and saved on a stack; in this case only one domain is detected. The threshold is decreased and checks are made for two conditions. The first is the appearance of a new region, which occurs at a threshold of 5 in the example. The centroids of new domains are added to the stack. The second condition is the merger of two domains, which occurs at threshold levels of 4 and 2. In this case, centroids of regions which were previously disconnected are stored as detected entities; otherwise, the centroids are ignored. In the example, all three peaks are detected and no arbitrarily specified constants are used.

The streamwise track diagram for one section of the jet shear layer is shown in Figure 8. Three complete cycles of the lowest subharmonic are required to cover the first six diameters of plume development. The jet instability frequency is 1/6 the initial shear-layer instability, and the 6 to 1 frequency reduction through vortex mergers can be deduced from these data. The six initial vortices pair to 4 by $x-x_o = d$, where x_o is the local lip position, and two vortical regions remain at 2d. Adaptive thresholding is unable to follow the final pairing and the results are ambiguous beyond 4d.

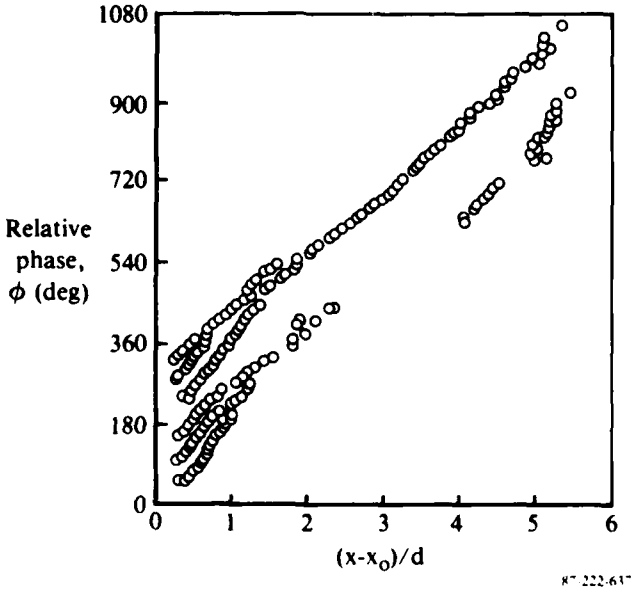

Fig. 8 Vortex tracks based on flow visualization; centroid tracking algorithm; azimuth $\psi = 180$ deg.

Vortical structures can easily be tracked near the nozzle lip where they are well-defined and nearly elliptic in cross-section. The strong distortion of the vortical domains that occurs in the later stages of jet development reduces the viability of peak-tracking in this region.

In the radial-integration algorithm, no attempt is made to track predetermined discrete entities within the shear layer. At each axial location, the total tracer concentration is integrated across the layer and after appropriate compensation and enhancement, the axial locations of vorticity concentrations can be determined. The complete processing scheme consists of the following steps:

1) Local histogram equalization of the raw image to enhance contrast.
2) Application of a mask at the average background intensity to remove light scattered by the nozzle.
3) Vertical line averages of the intensity in the upper and lower halves of the jet.
4) Subtraction of the overall average pixel intensity at each axial location.
5) Combination of the line averages into phase-versus-x diagrams.
6) Directional filtering to minimize phase-dependent contrast variations.
7) Histogram equalization to enhance overall contrast.

A typical result of this process is shown in Figure 9. The pixel intensities have been inverted so that tracer concentrations appear black. The initial development of the shear layer appears to be similar to that determined by the adaptive thresholding algorithm, but more detail is apparent in instances of incomplete pairing. The vortices labeled 1 through 3 coalesce into a single structure that persists for at least 3d from the nozzle lip. Vortex 4 appears to undergo partial pairings with 5 and 3, and 5 and 6 bypass one another before merging at 2d. Ultimately, only a single strong tracer concentration exists beyond 3d, although the diffusion of the scalar tracer masks the final coalescence.

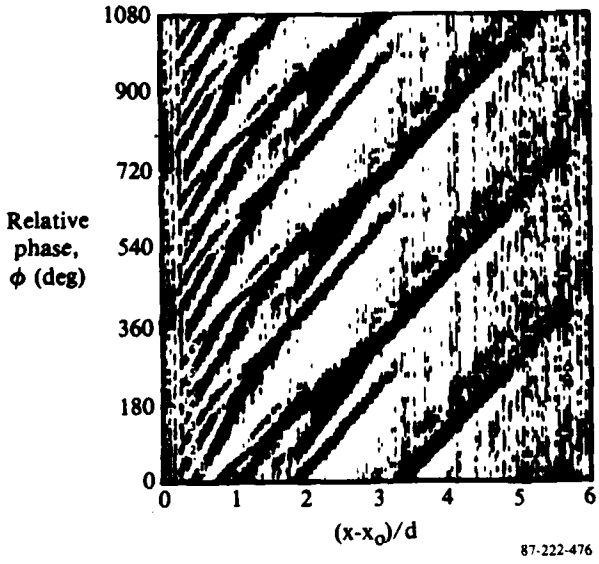

Fig. 9 Vortex tracks based on flow visualization; radial integration algorithm; azimuth $\psi = 180$ deg.

Phase-conditioned, two-component LDV data were obtained to compare with the visualization results because the distribution of seed material within the shear layer only approximately models the vorticity distribution. As discussed above, the acoustic excitation was different for the LDV and flow-visualization measurements, so only qualitative conclusions can be made. Data sets of 40,000 coincident bursts were obtained at each of 1406 grid points in the jet. A grid-generation routine was used to produce a Gaussian concentration of grid points in the shear layer, with a simultaneous linear stretch applied in the streamwise direction. Each cycle of the lowest subharmonic was subdivided into 64 parts, and the phase-conditioned vorticity was computed at each grid point.

The phase variation of vorticity integrated across the shear layer is shown in Figure 10. Dark areas correspond to domains of positive circulation. In this case the jet frequency is 1/8 the shear layer instability frequency. The acoustic excitation did not have a component at f_o, so the initial shear-layer rollup is difficult to detect. However, the streamwise evolution of the first through the third subharmonics is clearly visible. The results are qualitatively similar to those derived from the visualization, with the direct vorticity measurements better able to distinguish organized concentrations of vorticity up to 6d from the lip. The frequency at which the jet instability

is driven is greater than that in the flow visualization by a factor of 4/3, hence the apparent difference in the slope of the vortex tracks. Partial pairings are not evident, probably because the jet frequency is a 2^n (where n = 3) submultiple of the shear-layer instability frequency.

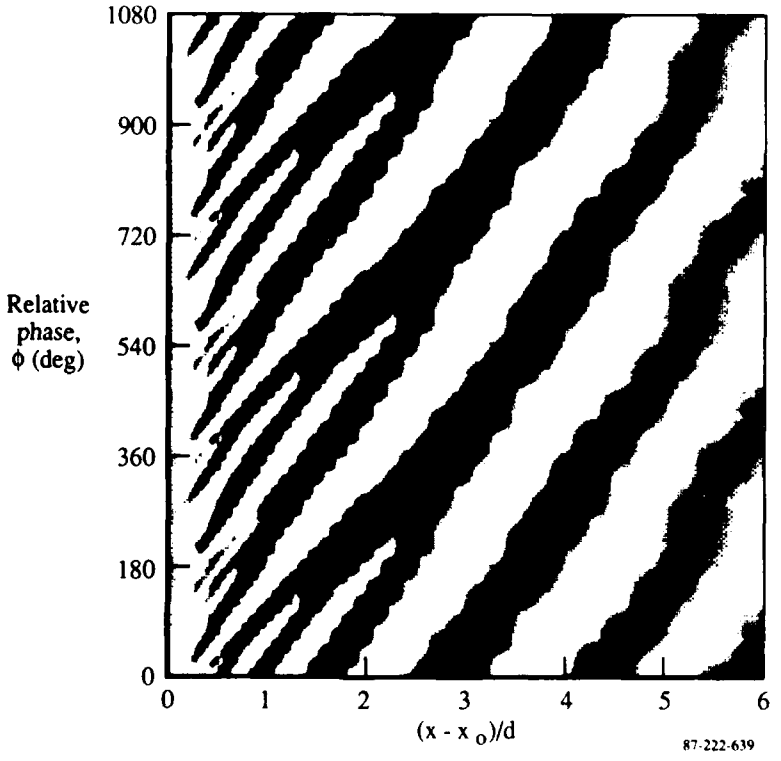

Fig. 10 Vortex tracks based on integrated vorticity from two-component LDV data; azimuth $\psi = 180$ deg.

The vortex track diagrams derived from the flow visualization have been recombined in Figure 11 into a physical description of the three-dimensional shear layer. Radial integrals of each of the sections taken at 19 azimuths around the jet have been combined at a constant value of the phase. In essence, the three-dimensional vortex structure has been unwrapped by image processing. Only 8 of the 32 total phases are shown here. As with the track diagrams, directional filtering and histogram equalization are used to de-emphasize azimuthal variations and increase contrast, respectively.

The inclined nozzle becomes a sinusoidal trailing-edge in the unwrapped representation. The most striking aspect of the processed data is that the

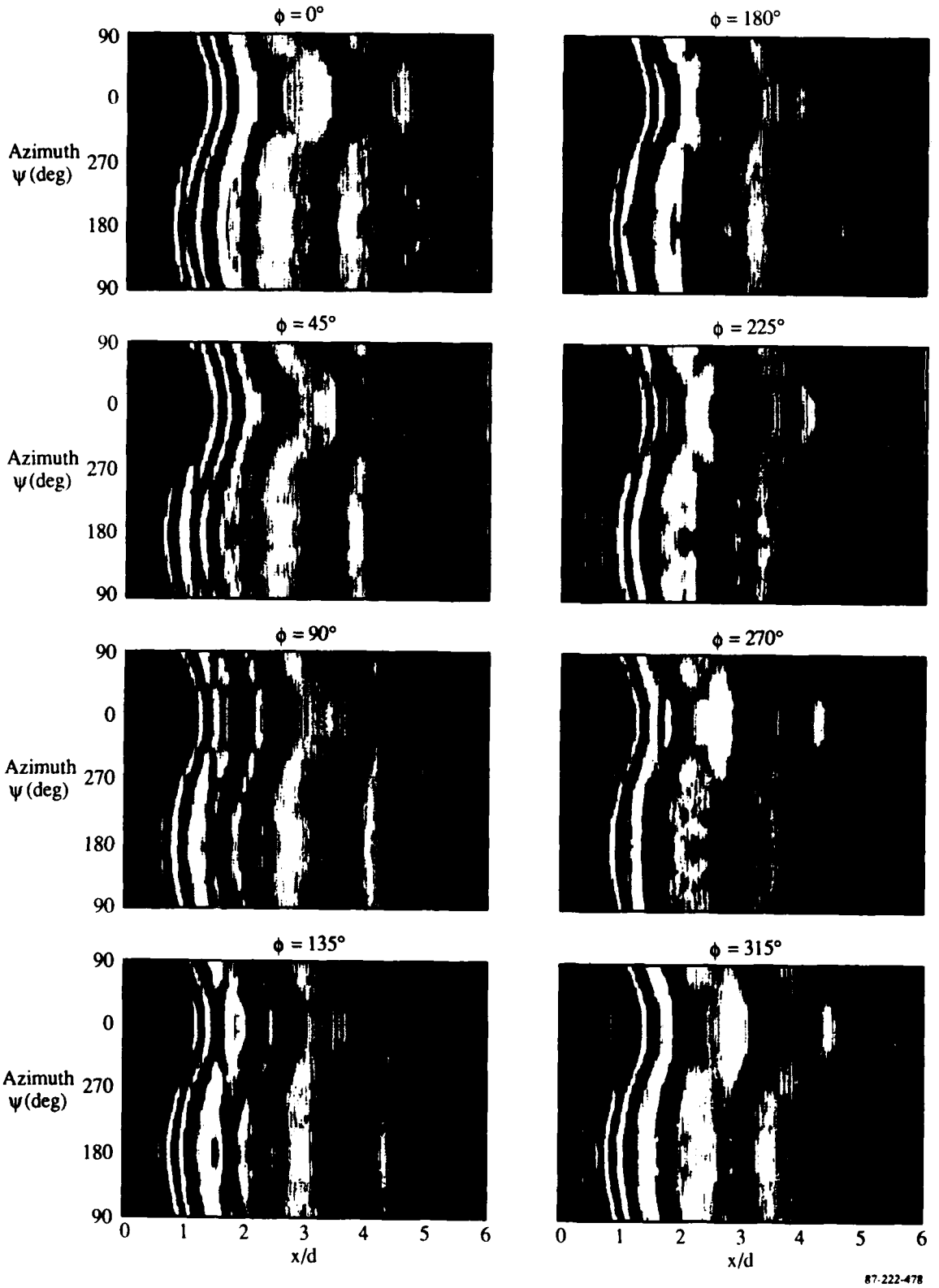

Fig. 11 Unwrapped vortex lines as a function of phase; black denotes smoke concentrations.

instability waves near the nozzle lip essentially form parallel to the trailing edge, but at $x/d = 4$ the structure is nearly axisymmetric. This is a direct axisymmetric analog of the two-dimensionalization of shear layers formed by splitter plates with a periodic distribution of tabs (Reference 4). The shear-layer reorganizes itself by partial pairing of the initially inclined ring vortices. At a relative phase of $\phi = 90°$, a vortex near $x/d = 1.5$ can be observed to be paired with an upstream vortex at azimuth $\psi = 0$ and a downstream vortex at $\psi = 180°$. At phase $\phi = 135°$, the vortex has been sufficiently distorted so that the segment which left the nozzle farthest downstream (azimuth $\psi = 0°$) is now farthest upstream, that is, the vortex has switched its angle of inclination. As the phase increases through $\phi = 225°$, the pairings become more complete with a filament of longitudinal vorticity connecting the rings near azimuth $\psi = 90°$.

3.4 Conclusions:

A technique has been developed in which flow-visualization images can be quantitatively processed to characterize complex three-dimensional vortex interactions in nonaxisymmetric jets. The three-dimensionally developing vorticity concentrations were labeled with a scalar tracer and illuminated with a phase-conditioned pulsed laser system. A direct tracking algorithm was found to be only partially successful, particularly in situations where partial pairing and vortex tearing occur. A radial-integration scheme provides a more general description of the shear layer when only axial development is required. Phase-conditioned two-component LDV measurements, which are impractical for routine use because of excessive acquisition and processing times, show qualitative agreement with the flow-visualization results when phase-conditioned vorticity is calculated.

The unwrapped images of the shear layer from the inclined-exit nozzle demonstrate a shear-layer growth mechanism that is consistent with the strong asymmetry documented in Reference 1. The initially inclined vortex system readjusts to become axisymmetric through partial pairings of the initially inclined ring vortex system. Portions of a vortex coalesce with upstream and downstream neighbors, ultimately producing a streamwise component of vorticity near $\psi = 90°$. Velocity measurements in Reference 1 have shown suppressed

shear-layer growth in this region, with significant spreading enhancement near $\psi = 0$ and 180°. The selective introduction of longitudinal vorticity thus appears to be an effective mechanism for controlling jet mixing.

4. TWO-STREAM MIXING LAYER FROM A SWEPT TRAILING EDGE

4.1 Background:

A series of experiments on jets from inclined-exit nozzles revealed several distinct patterns of shear-layer vortex formation, associated primarily with the nozzle exit-plane slant angle (References 1 and 2). It appeared that nozzle exits with low slant angles produced vortex-system constant-phase lines parallel to the nozzle exit, while high slant angles tended to generate growing instability waves approximately perpendicular to the flow direction. To study the basic properties of vortex development in shear layers originating from a slanted or swept separation edge, we have initiated the present study of a two-dimensional (in the mean), two-stream mixing layer produced by flow past a splitter plate with a swept trailing edge.

This section discusses the findings of the initial tests of the mixing-layer experiment.

4.2 Experimental Setup:

The experiments are being conducted in the MDRL Shear Flow Facility, a vertically arranged, closed-circuit, low-speed wind tunnel developed especially for studies of two-dimensional bounded and free shear layers. A large contraction ratio, smooth contraction fairing, and flow-conditioning elements (honeycomb and four screens) in the settling chamber ensure high-quality flow in the test channel. The test channel has glass windows along its full 5.5-m length for complete optical access to the flow.

The splitter-plate installation used to generate the two-stream mixing layer is shown schematically in Figure 12. The 1.27-cm-thick plate spans the full 91-cm width of the test channel and is sealed against the windows to prevent leakage because of the static-pressure difference across the plate. Positioned with its leading edge at the test channel entrance, the plate extends downstream 1.62 m at the mid-point of the trailing edge. The height of the high-speed (U_1) channel above the plate is 22.2 cm, while the lower-speed (U_2) channel is 14.0 cm high.

A variable velocity differential is created by developing a controllable pressure drop in the lower channel. The flow passes through two adjustable

and removable throttle plates and then through turbulence-damping screens to reduce disturbances generated by the throttle plates. Each throttle plate consists of a pair of matched perforated panels; lateral movement of one panel shifts its hole pattern relative to the other panel, changing the effective open area and hence the pressure drop across the throttle plate.

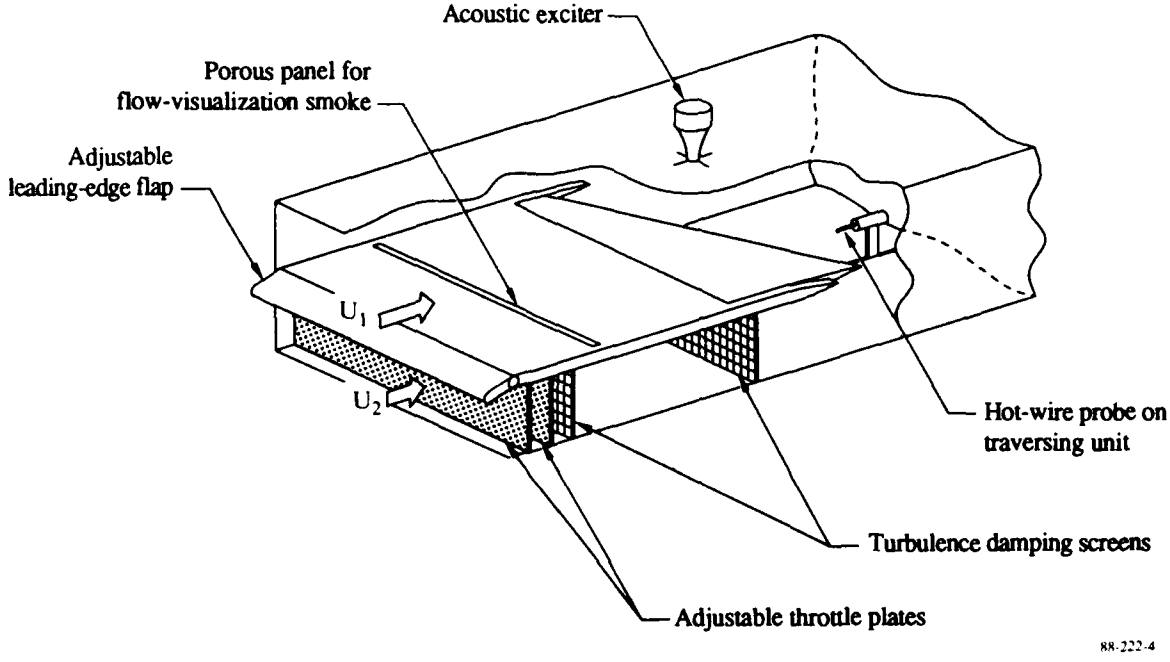

Fig. 12 Cutaway view of splitter plate with swept trailing edge insert in Shear Flow Facility test channel.

For shear-layer flow visualization, smoke (actually an aerosol of polyethylene glycol droplets) is bled into the upper-surface boundary layer through a porous panel in the plate surface. The resulting smoke layer downstream of the plate is illuminated by a strobe lamp above and behind the test channel.

Excitation of the mixing layer was accomplished acoustically via an audio driver in the test channel roof, above the mid-point of the splitter-plate trailing edge. We believe that the spanwise variation of phase (less than 3%) and amplitude along the trailing edge from the acoustic point source were acceptable for these preliminary experiments.

Initially, the splitter plate was fitted with an adjustable leading-edge flap to minimize local pressure gradients (and separation bubbles) resulting from leading-edge flowfield distortion associated with the difference in flow

rates above and beneath the splitter plate. Avoidance of such flow disturbances, which is necessary if laminar boundary layers are to be maintained on the plate surfaces, proved to be impossible. A satisfactory interim solution involved removing the flap and fitting a honeycomb and screen combination against the leading edge of the splitter plate. This arrangement permitted maintenance of laminar flow for a range of flow speeds and speed ratios. An extensively revised splitter-plate leading edge will be employed for the main body of experiments, to be conducted in early 1988.

Trailing-edge configurations studied are shown in Figure 13. Each trailing edge was sharp and symmetrical; the included angle at the trailing edge was approximately 5 degrees. For space and structure considerations, the 45-degree-sweep trailing edge was confined to the center half of the splitter-plate span, the rest of the span being taken up with unswept trailing-edge segments. Figure 13 also shows a set of white lines, laid out on the test channel floor perpendicular to the flow, that served as useful reference lines in flow-visualization work.

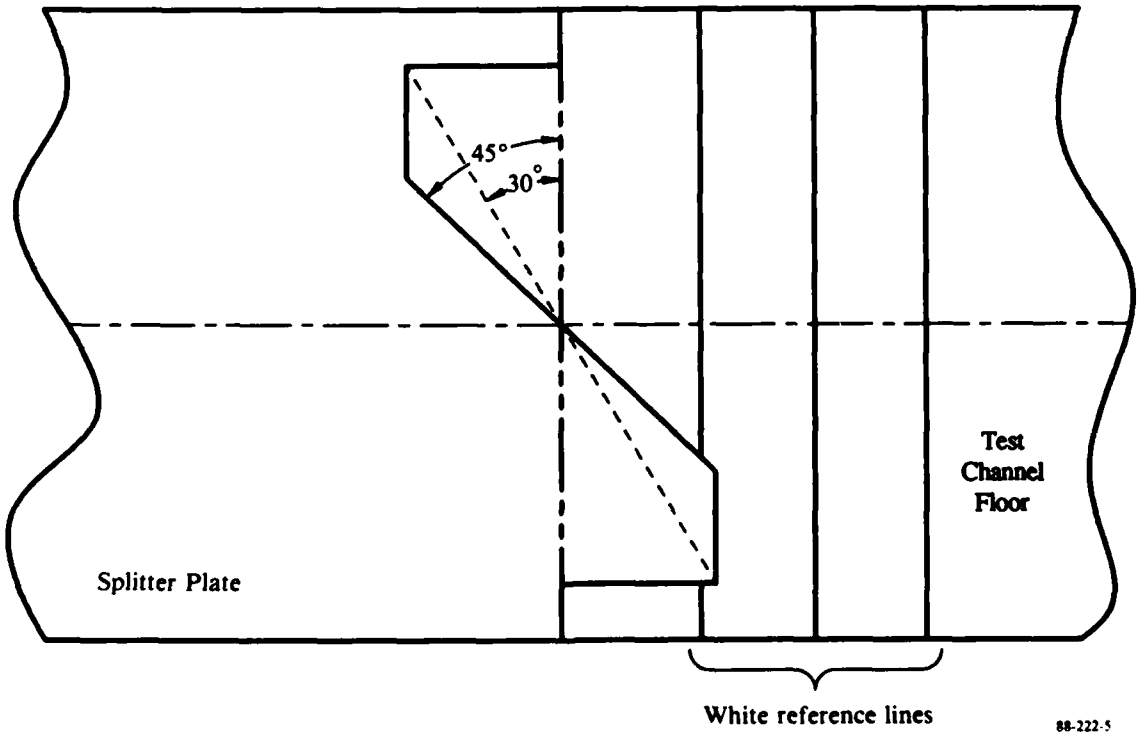

Fig. 13 Plan view showing splitter plate trailing-edge configurations for 0-, 30-, and 45-degree sweeps.

4.3 Results and Discussion:

Once the splitter-plate leading-edge problem had been satisfactorily resolved, it proved to be possible to obtain laminar trailing-edge separation up to a plate-length Reynolds number of 350,000 (corresponding to U_1 = 3.2 m/s). For this condition, mixing-layer velocity measurements at the trailing edge showed a characteristic laminar profile; upper-surface boundary-layer thickness at the trailing edge was about 2.0 cm.

The adjustable throttle plates were very effective, allowing a continuous range of speed ratios from U_1/U_2 = 1.4 (both throttle plates removed) to U_1/U_2 = 3.5 (maximum blockage from both throttle plates) to be achieved. Hot-wire measurements of streamwise turbulence intensity indicated that u'/U = 0.11% in the upper channel, and ranged from u'/U = 0.11% (minimum blockage) to u'/U = 0.19% (maximum blockage) in the lower channel. These levels were sufficiently low to have no apparent effect on the instability-wave and vortex-rollup processes in the laminar mixing layer. Hot-wire frequency spectra showed no significant peaks attributable to flow through the throttle plates.

Flow-visualization results with the unswept trailing edge showed that although some definite spanwise variation of phase and amplitude appeared, especially at the higher flow speeds (~3 m/s) and shear-layer excitation frequencies, the vortex-system development process was essentially two-dimensional. Sidewall boundary-layer-interaction effects were evident, such as a noticeable change in instability wavelength at the extremes of the smoke-layer span. However, these effects did not appear to influence instability-wave development away from the sidewall regions. (In fact, the original splitter-plate setup included transparent side plates to isolate the trailing-edge region of interest from the sidewall boundary layers, but these plates were found to promote boundary-layer transition on the splitter plate and were subsequently eliminated.)

Evidence of three-dimensional instability-wave interaction was seen in the nominally two-dimensional flow downstream of the 30-degree-sweep trailing edge. Figure 14 compares two flows that differ only in instability-wave excitation frequency. In these flow-visualization photos the view is directly from the side and somewhat above the mixing layer (note the reference lines on the channel floor). The shear layer in Figure 14(a), excited at f_x = 13 Hz,

develops instability waves that remain parallel to the trailing edge as they grow and roll up into discrete vortices. In Figure 14(b), however, the slightly shorter waves produced by the higher excitation frequency f_x = 15 Hz exhibit a "crossover" effect at about the middle of the smoke-sheet span: initially parallel to the plate trailing edge, each instability wave appears to break and reconnect so that every wave on the near side is connected to its downstream neighbor on the far side. As a result, the axes of the rolled-up vortices are swept at less of an angle than that of the trailing edge.

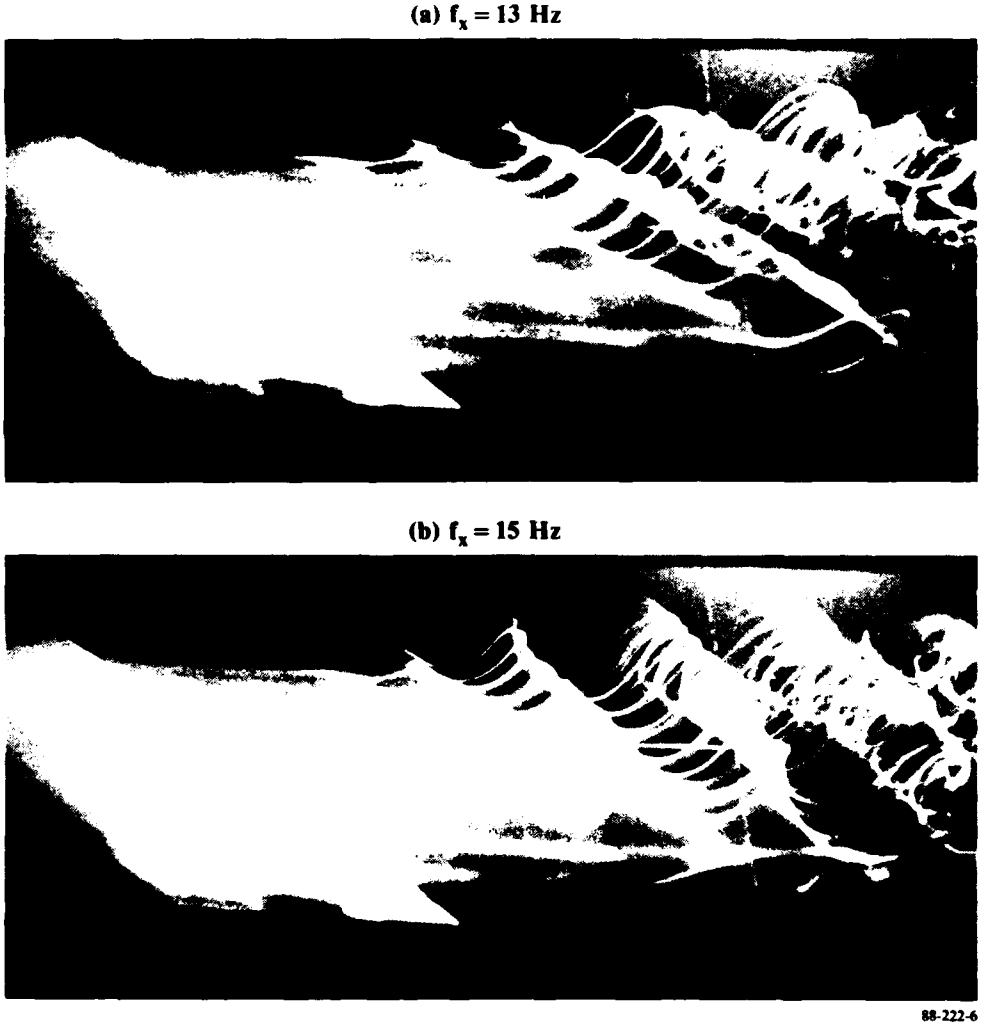

Fig. 14 Instability-wave development downstream of 30-degree sweep trailing edge for $U_1 \approx 1.5$ m/s, $U_1/U_2 \approx 1.8$.

Three-dimensional dynamic effects were much more prominent downstream of the 45-degree-sweep trailing edge. Figure 15 presents three views of mixing layers from the 45-degree trailing edge, again differing only in the excitation frequency applied to the layer. These views were obliquely downward and upstream, roughly parallel to the trailing edge. Note the unswept segments of the trailing edge, as well as the orientation of the reference lines on the test channel floor. The wave pattern in Figure 15(a), with no shear-layer excitation applied, is highly irregular. However, examination of the pattern reveals some superimposed organization into two wave families, one parallel to the swept trailing edge and the other perpendicular to the flow. (A videotape of this flow, illuminated stroboscopically at various frequencies, more clearly reveals the presence of the two wave families.) With excitation of f_x = 18 Hz [Figure 15(b)], the instability-wave and vortex-rollup pattern are definitely aligned with the 45-degree sweep of the trailing edge. But when the excitation frequency is increased to f_x = 24 Hz, the resulting wave pattern [Figure 15(c)] is clearly organized perpendicular to the flow direction. A side view of the same flow is shown in Figure 16, where excitation at the lower frequency [Figure 16(a)] produces waves parallel to the trailing edge, while excitation at f_x = 27 Hz yields waves transverse to the flow [Figure 16(b)].

It is instructive to observe that the frequencies associated with the swept and unswept instability-wave families, 18 Hz and 24-27 Hz, respectively, are related in such a way that the wavelengths of the two families are the same. If λ = wavelength, then the wave spacing in the stream direction is $L = \lambda/\cos\Lambda$, where Λ is the sweep angle of the wave system. For waves convecting streamwise with speed U_c,

$$U_c = fL = f\lambda/\cos\Lambda \ .$$

Using $(\ )_1$ to denote the swept waves and $(\ )_2$ the transverse waves, and assuming U_c to be the same for both sets,

$$U_c = f_1\lambda_1/\cos\Lambda_1 = f_2\lambda_2/\cos\Lambda_2 \ .$$

(a) $f_x = 0$ Hz

(b) $f_x = 18$ Hz

(c) $f_x = 24$ Hz

88-222-7

Fig. 15 Shear-layer vortex formation behind 45-degree sweep trailing edge at $U_1 = 2.25$ m/s, $U_1/U_2 \approx 1.9$.

Since $\Lambda_2 = 0$,

$$\frac{f_1}{f_2} = \frac{\lambda_2}{\lambda_1} \cos \Lambda_1 \ .$$

In the present case

$$\frac{f_1}{f_2} = \frac{18 \text{ Hz}}{24\text{-}27 \text{ Hz}} = 0.7 \ ,$$

$$\cos\Lambda_1 = 0.707,$$

and hence $\lambda_1 = \lambda_2$.

(a) $f_x = 18$ Hz

(b) $f_x = 27$ Hz

88-222-8

Fig. 16 Side view of same flow as in Fig. 15 (U_1=2.25 m/s, U_1/U_2~1.9).

4.4 Summary:

A preliminary exploration of instability-wave development in the laminar mixing layer behind a swept trailing edge has been conducted. This "shake-down" test has identified aspects of the experimental approach that will benefit from improvement prior to the main series of experiments to be performed in 1988. The test demonstrated the effectiveness of adjustable perforated-panel throttle plates in providing a variable flow-speed ratio across the mixing layer with only a modest increase in freestream turbulence intensity.

For swept trailing edges, flow-visualization studies clearly showed two distinct, interacting families of instability waves, one parallel to the trailing edge and the other perpendicular to the flow. Acoustic excitation of the mixing layer allowed substantial enhancement of either set of waves, depending on excitation frequency. Wavelengths of the two wave families appeared to be the same. The appearance of two interacting wave families was very pronounced for the 45-degree-sweep trailing edge, but was only marginally evident in the 30-degree-sweep case.

5. PRESENTATIONS

The following MDRL presentations have resulted from the subject contract.

1. R. W. Wlezien, "Asymmetric Vortex Interactions in Nonaxisymmetric Jets," Bull. Am. Phys. Soc. 32, 10 (1987).
2. R. W. Wlezien, "Quantitative Visualization of Acoustically Excited Jets," AIAA Paper 88-0499, 1988. Presented at the 26th Aerospace Sciences Meeting, Reno, Nevada, 13 January 1988.
3. V. Kibens, R. W. Wlezien, F. W. Roos, and J. T. Kegelman, "Trailing Edge Sweep and Three-Dimensional Vortex Interactions in Jets and Mixing Layers." Submitted for presentation at the Symposium on Fluid Dynamics of Three Dimensional Turbulent Shear Flows and Transition to be held in Turkey, 3-6 October 1988.

6. REFERENCES

1. Wlezien, R. W. and Kibens, V., "Passive Control of Jets with Indeterminate Origins," AIAA J., Vol. 24, August 1986, pp. 1263-1270.
2. Kibens, V. and Wlezien, R. W., "Active Control of Jets from Indeterminate-Origin Nozzles," AIAA Paper 85-0542, 1985.
3. Kegelman, J., "A Flow-Visualization Technique for Examining Complex Three-Dimensional Flow Structures," Proc. 10th Symposium on Turbulence, University of Missouri-Rolla, September, 1986.
4. Breidenthal, R., "Response of Plane Shear Layers and Wakes to Strong Three-Dimensional Disturbances," The Physics of Fluids, Vol. 23, October, 1980, pp. 1929-1934.

END

DATE

FILMED

8-88

DTIC